JOURNAL OF MATERIALS SCIENCE 28 (1993) 5744–5752

X-ray diffraction and Fourier transform–infrared analysis of the rust formed by corrosion of steel in aqueous solutions

S. MUSIĆ, M. GOTIĆ, S. POPOVIĆ*
*Ruđer Bošković Institute, PO Box 1016, 41001 Zagreb, *and also Department of Physics, Faculty of Science, University of Zagreb, PO Box 162, 41001 Zagreb, Republic of Croatia*

Chemical and structural properties of the rust formed by corrosion of steel in aqueous solutions were studied by X-ray diffraction and Fourier transform infrared (FT–IR) spectroscopy. The corrosion products of steel were generated in aqueous solutions of different electrolyte compositions at room temperature (20 °C) or in an autoclave at 120 °C. X-ray diffraction analysis showed the presence of different oxide phases in the rust, such as lepidocrocite, magnetite, ferrihydrite, goethite and haematite. In all samples, the presence of an amorphous fraction was detected. Ferrihydrite was detected only in the rust samples formed at 120 °C. The characteristic properties of the FT–IR spectrum of the ferrihydrite component in the rust were investigated. Phase compositions of the corrosion products depended on the formation temperature and the electrolyte composition of the aqueous solutions. The influence of chloride, nitrate or sulphate anions on the phase composition of the rust is discussed.

1. Introduction

The phase composition of the corrosion products of steel in an aqueous medium depends on different parameters, such as temperature, pH and the oxygen content. The surface treatment of steel and the presence of various ions in aqueous solution may also affect the phase composition of the corrosion products of steel. Numerous investigations showed the presence of different oxide phases in the rust, such as $Fe(OH)_2$, $Fe(OH)_3$, α-FeOOH, β-FeOOH, γ-FeOOH, δ-FeOOH, α-Fe_2O_3, γ-Fe_2O_3 and Fe_3O_4. Significant discrepancies, concerning the chemical and structural properties of the rust formed by the corrosion of the steel in an aqueous medium, can be found in the literature. The crystallinity, stoichiometry, particle size and morphology of the oxide components in the rust may vary significantly. The limitations of experimental techniques can be also the source of errors in determination of the phase composition of the rust. The renewed investigations performed with advanced spectroscopic techniques showed that in many cases the phase composition of the rust differs from the phase composition found by the traditional techniques.

Mössbauer spectroscopy was used to follow the chemical composition of the rust formed on the steel surface after atmospheric exposure of steel for different times at Bethlehem, PA, USA [1]. Lepidocrocite, γ-FeOOH, was determined as the initial corrosion product, which converted with time to a mixture of goethite, α-FeOOH, and maghaemite, γ-Fe_2O_3. After a prolonged time, estimated at 25 years, the rust contained more than 90% γ-Fe_2O_3. The similarity between the composition of the corrosion products and precipitates formed from $FeSO_4$ solutions, under mild acidic conditions at 90 °C, suggested that sulphate anions played a dominant role in the atmospheric corrosion experiments. This was supported by the fact that the Bethlehem area in Pennsylvania is rich in SO_2/SO_3, due to iron works and a coke factory.

Mössbauer spectroscopic analysis of the rust, formed during the simulation of atmospheric corrosion in the presence of sulphate anions, showed the presence of γ-FeOOH and ferrihydrite after 3 days [2]. Traces of γ-Fe_2O_3 were present after 6 weeks with a tendency of increasing γ-Fe_2O_3 fraction with corrosion time. It was shown that the sequence of oxide phases present as a function of time was the same in the case of the atmospheric corrosion and in the laboratory corrosion experiments, in which the steel surface was contaminated with a corresponding salt, with the exception of the phases formed during the very early stages of the corrosion process. The importance of the wet/dry cycles during the corrosion process was also discussed.

Electrochemical measurements, Auger and Mössbauer spectroscopy were applied to investigate the corrosion resistance of steel in water after abrasive blasting with alumina [3]. The analysis showed that Al_2O_3 particles were incorporated into the steel surface after abrasive blasting. The formation of iron oxide film with structurally incorporated Al^{3+} ions was suggested. This oxide film was assumed to be a poorer catalyst for the oxygen reduction reaction and more resistant to anodic attack. Abrasive blasting of steel with fine oxide powder may be used for the chemical modification of surfaces.

0022–2461

The corrosion of steel in an aqueous medium is a process of electrochemical nature, and the result of this process is the formation of rust, which exhibits colloidal properties. The mechanism of rust formation, during corrosion of steel in an aqueous medium, can be followed to a certain stage by the analogy with the precipitation of oxides from Fe(II)- or Fe(III)-salt solutions. The usefulness of these investigations increases as the conditions in the laboratory experiments approach those in actual corrosion processes.

Mössbauer spectroscopy was used to investigate the precipitates formed by hydrolysis of Fe^{3+} ions in solution containing nitrate, chloride or sulphate anions [4]. On the basis of the experimental results, it was concluded that the hydrolysis of Fe^{3+} in nitrate and chloride solutions was characterized by the formation of monomers and dimers of Fe^{3+} ions and further by the formation of polymeric species. The polymers formed in the nitrate solutions were not presumed to include the nitrate ions in the polymer chain, while the polymers formed in the chloride solution contained some chloride ions instead of the OH^- ion. The next step in the precipitation process was the formation of oxybridges and the development of α-FeOOH or β-FeOOH structures. α-FeOOH transformed to α-Fe_2O_3 by an internal crystallization process. In sulphate solutions, the formation of $FeSO_4^+$ complex suppressed the polymerization process and the formation of oxyhydroxides and oxides. Basic Fe(III)-sulphates were formed instead.

Musić *et al.* [5, 6] studied the chemical composition, crystallinity, stoichiometry and nuclear magnetic properties of oxide precipitates formed from $FeSO_4$ solutions. They found that the chemical and structural properties of the iron oxides formed were strongly dependent on the $[Fe^{2+}]/[OH^-]$ concentration ratio at the beginning of the precipitation process, the rate of oxygenation, the time of precipitation, the temperature and the kind of alkali added (NH_4OH or NaOH).

Chemical and structural properties of oxide precipitates, formed from $FeSO_4$ solutions containing urea, were investigated using X-ray diffraction and ^{57}Fe Mössbauer spectroscopy [7]. The hydrolysis of urea at elevated temperature was used for the generation of OH^- ions during the precipitation process. The phase analysis of precipitates showed the presence of different oxide phases, such as goethite, lepidocrocite, heamatite and magnetite, and in one sample a small amount of siderite. Only substoichiometric magnetite, $Fe_{3-x}O_4$, was detected. Significant differences in the Mössbauer spectra of goethite were observed, owing to different particle sizes and the degree of crystallinity and/or different content of structurally bonded water. The correlation between the Mössbauer spectra of precipitated goethite and goethite formed during the atmospheric corrosion of the steel was discussed.

In the present paper, we report the results of analysis of the corrosion products of steel formed in aqueous solutions under different experimental conditions. The corrosion experiments were performed in the presence of different anions in order to determine their influence on the chemical and structural properties of the rust. X-ray diffraction (XRD) and Fourier transform–infrared (FT–IR) spectroscopy were used as experimental techniques. FT–IR spectroscopy is characterized with a better sensitivity and resolution in relation to conventional IR spectroscopy.

2. Experimental procedure

Analar grade chemicals and doubly distilled water were used. Cold rolled low carbon steel, JUS-Č0146 (C_{max} = 0.12%, Mn_{max} = 0.50%, P_{max} = 0.040%, S_{max} = 0.040%) was cut into the coupons with dimensions 60 mm × 100 mm. Experiments were performed at room temperature (20 °C) and at 120 °C. During the corrosion process, the experimental systems were not in contact with oxygen from air. Autoclaves were used for the investigation of corrosion of steel at 120 °C. Experimental conditions for the preparation of nineteen corrosion products of steel, S-1–S-19, are given in Table I. The adherent corrosion layer formed on the steel surface was scraped from the steel foil and, together with the non-adherent corrosion layer, was cleaned with doubly distilled water from mother liquor using a SORVALL RC2-B superspeed centrifuge (up to 20 000 r.p.m.). The corrosion products were dried in vacuum at room temperature.

X-ray powder diffraction measurements were performed at room temperature using a Philips counter diffractometer with monochromatized Cu$K\alpha$ radiation (graphite monochromator).

FT–IR spectra were recorded at room temperature using a spectrometer 1720-x produced by Perkin–Elmer. Samples were pressed in discs using spectroscopically pure KBr. FT–IR spectra of standard iron oxides were also recorded. The origin of standard iron oxides was described in a previous paper [5].

TABLE I Experimental conditions for the preparation of corrosion products of steel; samples S-1–S-19

Corrosion product	Chemical composition of solution	Corrosion time (h)	Solution temperature (°C)
S-1	Doubly distilled water	336	20
S-2	Doubly distilled water	48	120
S-3	0.05 M NaCl	816	20
S-4	0.50 M NaCl	816	20
S-5	5.00 M NaCl	816	20
S-6	0.50 M NH_4Cl	360	20
S-7	3.50 M NH_4Cl	384	20
S-8	3.50 M NH_4Cl	48	120
S-9	0.50 M $NaNO_3$	336	20
S-10	0.50 M $NaNO_3$	571	20
S-11	5.00 M $NaNO_3$	336	20
S-12	0.50 M $NaNO_3$	120	120
S-13	0.50 M $NaNO_3$	240	120
S-14	3.50 M $NaNO_3$	66	120
S-15	3.50 M $NaNO_3$	192	120
S-16	0.10 M Na_2SO_4	690	20
S-17	0.50 M Na_2SO_4	718	20
S-18	0.10 M Na_2SO_4	239	120
S-19	0.50 M Na_2SO_4	120	120

3. Results

3.1. X-ray diffraction

Iron hydroxides, oxyhydroxides and oxides are typical components of the rust formed by the corrosion of steel in an aqueous medium or during the atmospheric corrosion of steel. Their crystallographic data are given in Table II [8].

The results of XRD phase analysis of the corrosion products of steel are given in Table III. Corrosion product S-1, formed on the steel surface in doubly distilled water at 20 °C, is a mixture of lepidocrocite, magnetite and amorphous fraction, AF. The amorphous fraction was also detected in all studied corrosion products, and its presence was indicated by an increased background intensity in a given angular region.

Corrosion product S-2, formed on the steel surface in doubly distilled water at 120 °C contained magnetite as the dominant component and also ferrihydrite, FH, and goethite. Corrosion products S-3, S-4 and S-5 were formed at 20 °C by the corrosion of steel in 0.05, 0.50 and 5.00 M NaCl, respectively. The results of XRD phase analysis indicated the influence of NaCl concentration on the phase composition of the rust. Corrosion product S-3 consisted of magnetite showing broadened diffraction lines, due to the small crystallite sizes. In corrosion products S-4 and S-5, in addition to magnetite, lepidocrocite was also detected. Magnetite was dominant in corrosion product S-4, while lepidocrocite was dominant in corrosion product S-5. The fraction of lepidocrocite increased with the concentration of NaCl.

Corrosion products S-6, S-7 and S-8 were formed in aqueous solutions containing NH_4Cl. Corrosion product S-6, formed in 0.50 M NH_4Cl at 20 °C, was a mixture of lepidocrocite and magnetite, while corrosion product S-7, formed in 3.50 M NH_4Cl at the same temperature, contained lepidocrocite. Corrosion product S-8, formed in 3.50 M NH_4Cl at 120 °C, consisted of haematite, goethite and ferrihydrite. The diffraction lines of these oxides were broadened.

Corrosion products S-9, S-10 and S-11, formed in 0.50 or 5.00 M $NaNO_3$ solution at 20 °C, contained magnetite and lepidocrocite. Corrosion products S-12, S-13, S-14 and S-15, formed in $NaNO_3$ solutions at 120 °C, consisted mostly of an amorphous component with a very small fraction of ferrihydrite, FH, and only in corrosion product S-13, of magnetite and haematite. Corrosion products of steels S-16, S-17, S-18 and S-19 were generated in aqueous solutions containing Na_2SO_4. In corrosion products S-16 and S-17, formed at 20 °C, lepidocrocite, magnetite and goethite or haematite were detected. However, in corrosion products S-18 and S-19, formed at 120 °C, lepidocrocite was not detected. In these corrosion products, magnetite was the dominant component, while ferrihydrite and goethite were additional oxide phases.

3.2. FT–IR spectroscopy

FT–IR spectra of corrosion products S-1 and S-2 are shown in Fig. 1. The presence of lepidocrocite in corrosion product S-1 was detected on the basis of characteristic IR bands at 1023 and 747 cm^{-1}. The standard lepidocrocite showed sharp IR bands at 1023 and 752 cm^{-1}. The broad IR band with transmission minimum at 3162 cm^{-1} was the result of OH stretching within the bulk of iron (III) oxyhydroxide, while the IR band at 1637 cm^{-1} corresponded to

TABLE II Crystallographic data for iron hydroxides, oxyhydroxides and oxides, which can appear as components of the rust [8]

Compound	Mineral name	Space group or crystal system	Unit-cell parameters (nm) at room temperature	Formula units per unit cell	JCPDS PDF Card no.
$Fe(OH)_2$		$P\bar{3}m1$ (164)	$a = 0.3258$ $c = 0.4605$		13–89
$Fe(OH)_3$		Cubic	$a = 0.8370$		22–346
$Fe_5O_7(OH)$ 4 H_2O	Ferrihydrite	Hexagonal	$a = 0.508$ $c = 0.940$	1	29–712
α-FeOOH	Goethite	$Pbnm$ (62)	$a = 0.4608$ $b = 0.9956$ $c = 0.30215$	4	29–713
β-FeOOH	Akaganeite	Tetragonal	$a = 1.048$ $c = 0.3023$	8	13–157
γ-FeOOH	Lepidocrocite	$Amam$ (63)	$a = 0.3880$ $b = 1.254$ $c = 0.3070$	4	8–98
α-Fe_2O_3	Haematite	$R\bar{3}c$ (167)	$a = 0.50340$ $c = 1.3752$	6	13–534
γ-Fe_2O_3	Maghemite	Tetragonal, spinel-like structure, with cubic sub-cell $a = 0.834$ nm	$a = 0.834$ $c = 2.502$		25–1402
Fe_3O_4	Magnetite	$Fd\bar{3}m$ (227)	$a = 0.8396$	8	19–629

TABLE III The results of XRD phase analysis of the corrosion products generated in aqueous solutions, S-1–S-19

Corrosion product	Phase composition [a] (approximate molar fraction)
S-1	γ-FeOOH + Fe_3O_4 + AF (3/5) (2/5)
S-2	Fe_3O_4 + FH[b] + α-FeOOH[b] + AF (3/6) (2/6) (1/6)
S-3	Fe_3O_4[b] + AF
S-4	Fe_3O_4 + γ-FeOOH + AF (2/3) (1/3)
S-5	γ-FeOOH + Fe_3O_4 + AF (3/4) (1/4)
S-6	γ-FeOOH + Fe_3O_4 + AF (2/3) (1/3)
S-7	γ-FeOOH[b] + AF
S-8	α-Fe_2O_3[b] + α-FeOOH[b] + FH[b] + AF (3/6) (2/6) (1/6)
S-9	Fe_3O_4 + γ-FeOOH[b] + AF (2/3) (1/3)
S-10	γ-FeOOH[b] + Fe_3O_4[b] + AF (> 9/10) (< 1/10)
S-11	Fe_3O_4 + γ-FeOOH[b] + AF (1/2) (1/2)
S-12	AF + FH[c]
S-13	AF + FH[c] + Fe_3O_4[c] + α-Fe_2O_3[c]
S-14	AF + FH[b,c]
S-15	AF + FH[c]
S-16	γ-FeOOH + Fe_3O_4 + α-FeOOH + AF (3/6) (2/6) (1/6)
S-17	γ-FeOOH[b] + Fe_3O_4 + α-Fe_2O_3[c] + AF (5/6) (1/6)
S-18	Fe_3O_4 + FH[b] α-FeOOH[b] + AF (3/5) (1/5) (1/5)
S-19	Fe_3O_4 + FH[b] + α-FeOOH[b] + AF (3/5) (1/5) (1/5)

[a] FH = ferrihydrite, $Fe_5O_7(OH)\cdot 4H_2O$, AF = an amorphous fraction.
[b] Diffraction line broadening due to small crystallite sizes.
[c] Very faint diffraction lines.

molecular water in hydrogen-bonded association. The presence of magnetite in corrosion product S-1 was detected on the basis of a broad IR band at 579 cm^{-1}. The FT–IR spectrum of a substoichiometric magnetite $Fe_{3-x}O_4$ showed a strong IR band at 575 cm^{-1}, a band at 385 cm^{-1} and shoulders at 668 and 442 cm^{-1}. The main characteristics of the FT–IR spectrum of corrosion product S-2 were broad bands at 3402 and 914 cm^{-1}, a broad band with transmission minima at 574 and 476 cm^{-1} and a shoulder at 614 cm^{-1}. Magnetite can be detected on the basis of the IR band at 574 cm^{-1}. X-ray diffraction showed the presence of goethite in corrosion product S-2. However, no contribution of α-FeOOH to the FT–IR spectrum could be observed, because the IR bands characteristic for α-FeOOH at 893 and 796 cm^{-1} were overlapped by a broad band at 914 cm^{-1}. The shoulder at 614 cm^{-1} may be related to the IR band at 633 cm^{-1}, observed for a standard goethite sample, only if the results of the

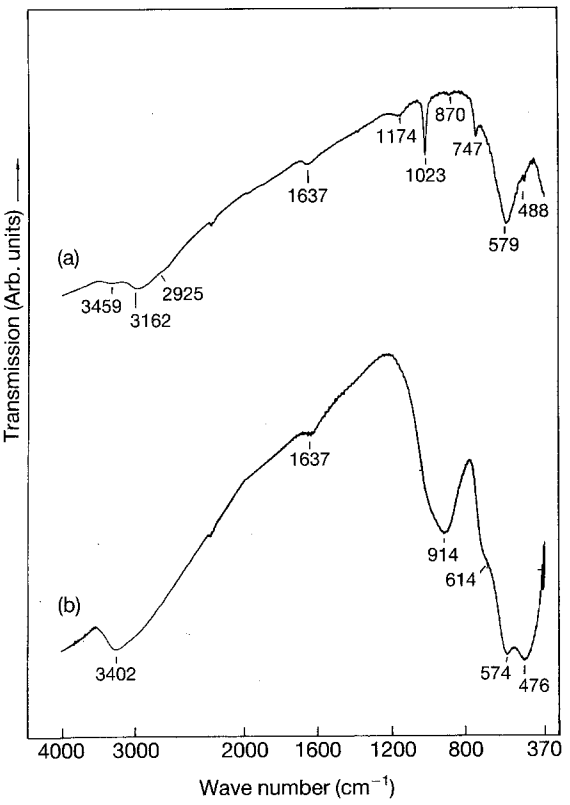

Figure 1 FT–IR spectra of corrosion products (a) S-1 and (b) S-2.

phase analysis, obtained by a technique complementary to FT–IR spectroscopy, are known.

In order to solve the origin of the IR band at 914 cm^{-1} recorded for corrosion product S-2, amorphous iron(III) hydroxide was precipitated from $Fe(NO_3)_3$ solution. The hydroxide precipitate was cleaned several times with doubly distilled water to remove neutral electrolyte. The separation of solid phase from liquid phase was performed using the superspeed centrifuge. Hydroxide precipitate was dried in a vacuum at room temperature. XRD analysis showed that this sample was completely amorphous. The FT–IR spectrum of amorphous iron(III) hydroxide, shown in Fig. 2, indicated a characteristic region at 3371 cm^{-1}, then the region with IR bands 1624, 1507, and 1360 cm^{-1}, a very weak IR band at 1044 cm^{-1} and a very strong IR band with transmission minima at 566 and 448 cm^{-1}. However, the broad and pronounced band near 914 cm^{-1} was not observed in the FT–IR spectrum of amorphous iron(III) hydroxide. Because the XRD pattern of corrosion product S-2 showed the presence of ferrihydrite, the IR band at 914 cm^{-1} observed for the same corrosion product, can be ascribed to ferrihydrite. This type of IR band was always present in the FT–IR spectra of all corrosion products generated at 120 °C, for which XRD showed the presence of ferrihydrite. Depending on the origin of the corrosion products, the IR band at 914 cm^{-1} was shifted to higher wave numbers, up to $\simeq$ 1000 cm^{-1}.

Fig. 3 shows FT–IR spectra of corrosion products S-3, S-4 and S-5, which were generated by the corrosion of steel in NaCl solutions. For corrosion product S-3, the IR bands at lower wave numbers, with very

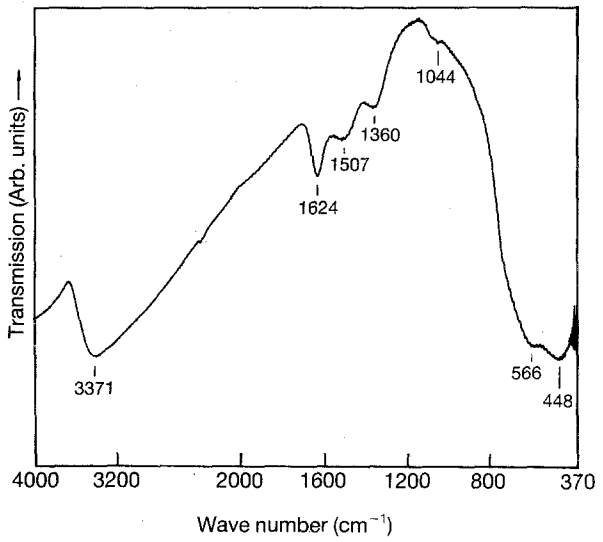

Figure 2 FT–IR spectrum of iron (III) hydroxide.

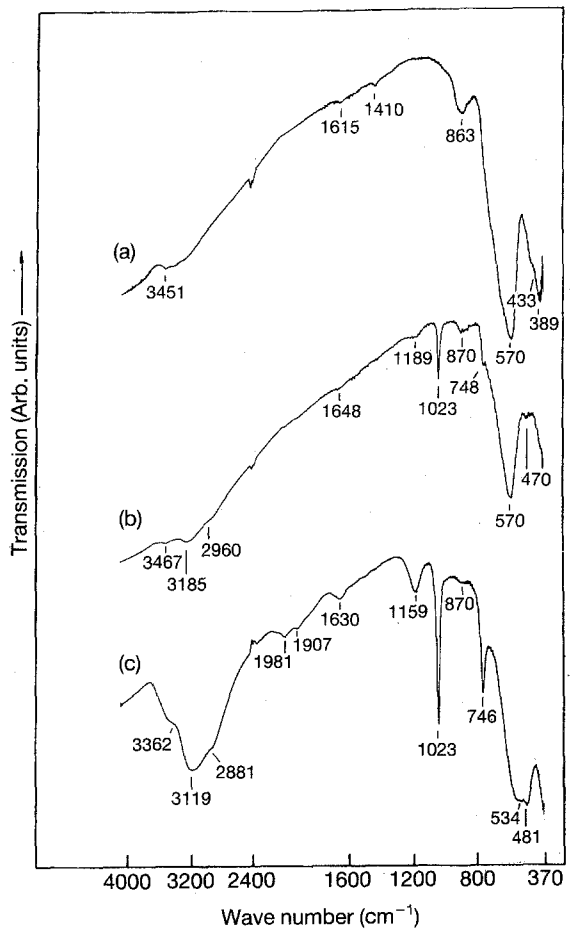

Figure 3 FT–IR spectra of corrosion products (a) S-3, (b) S-4 and (c) S-5.

strong band at 570 cm^{-1} can be ascribed to magnetite. The FT–IR spectrum of corrosion product S-4 indicated that magnetite was the dominant component of the rust. The presence of lepidocrocite could be proved on the basis of a sharp IR band at 1023 cm^{-1} and a shoulder at 748 cm^{-1}. The relative intensities of these IR bands were bigger in the FT–IR spectrum of corrosion product S-5 than in the FT–IR spectrum of corrosion product S-4. The FT–IR spectrum of corrosion product S-5 also showed an IR band at 481 cm^{-1}, which was observed in the cases when lepidocrocite was the dominant component of the rust. Also, as the fraction of magnetite in the rust increased, its characteristic IR band at 570 cm^{-1} shifted to 534 cm^{-1} (from S-3–S-5).

FT-IR spectra of corrosion products S-6, S-7 and S-8, prepared in NH_4Cl solutions are shown in Fig. 4. Lepidocrocite was the dominant component of the rust in S-6 and S-7. Magnetite can be detected only on the basis of the shoulder at 560 cm^{-1}. That shoulder did not appear in the FT–IR spectrum of corrosion product S-7, thus indicating the absence of magnetite in accordance with XRD results. The FT–IR spectrum of corrosion product S-8 showed a very strong and broad band with tranmission minima at 568 and 476 cm^{-1}. The XRD pattern of corrosion product S-8 showed that haematite was the dominant component. However, IR bands at 568 and 476 cm^{-1} cannot be ascribed to haematite only on the basis of FT–IR measurements. In this region of the IR spectrum (400–600 cm^{-1}) there is also a strong influence of vibration frequencies originating from magnetite, ferrihydrite or lepidocrocite. The FT–IR spectrum of corrosion product S-8 also indicated the presence of goethite (bands at 906 and 803 cm^{-1}). Broadening of the band at 906 cm^{-1} was probably the result of low crystallinity and the small crystallite sizes of goethite.

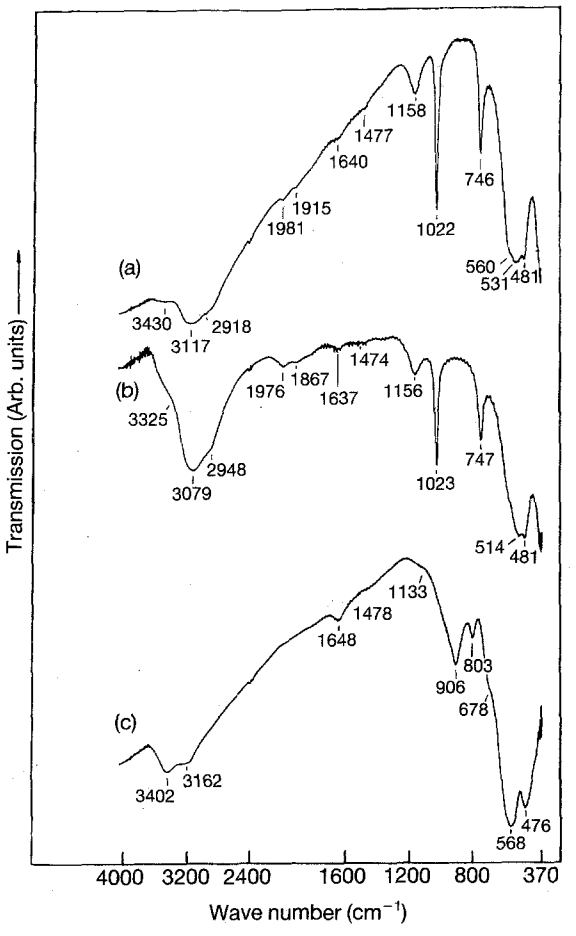

Figure 4 FT–IR spectra of corrosion products (a) S-6, (b) S-7 and (c) S-8.

FT–IR spectra of corrosion products S-9, S-10 and S-11 showed the presence of magnetite and lepidocrocite, as crystalline phases, which was in accordance with XRD results.

Fig. 5 shows FT–IR spectra of corrosion products of S-12, S-13, S-14 and S-15, which were generated by the corrosion of steel in $NaNO_3$ solutions at 120 °C. The main characteristics of these spectra were very broad IR bands at 3402–3431, 975–1019 and 471–443 cm^{-1}. XRD showed that these corrosion products, S-12–S-15, consisted dominantly of an amorphous fraction and ferrihydrite. The strong and broad band at 975–1019 cm^{-1} was ascribed to ferrihydrite, having probably very small crystallite sizes and low crystallinity. The amorphous fraction can be ascribed to iron(III) hydroxide, and/or other oxide phases. IR bands of low intensity in the regions of 1474–1465 and 1403–1388 cm^{-1}, shown in FT–IR spectra of samples S-12, S-13, S-14 and S-15, could be ascribed to residual nitrates. Sharp IR bands at 2921 and 2851 cm^{-1}, observed for sample S-14, can be ascribed to residual C_2H_5OH, which was used in the cleaning procedure of the corrosion products.

Fig. 6 shows FT–IR spectra of corrosion products S-16, S-17, S-18 and S-19, which were generated during corrosion of steel in Na_2SO_4 solutions. FT–IR spectra of corrosion products S-18 and S-19 showed very strong and broad bands at 1013 and 989 cm^{-1}, respectively. These IR bands could be ascribed to ferrihydrite. Ferrihydrite was also detected in corrosion products S-18 and S-19 using XRD.

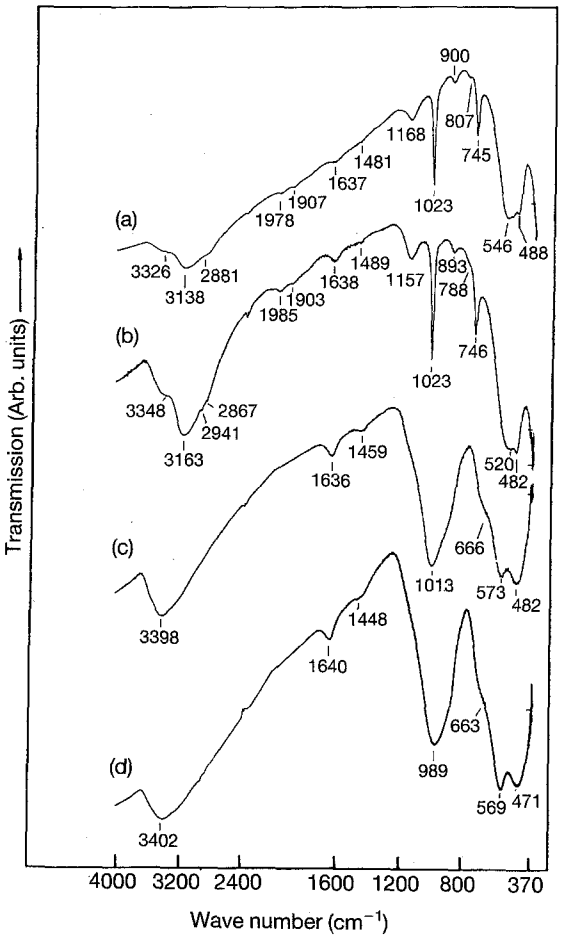

Figure 6 FT–IR spectra of corrosion products (a) S-16, (b) S-17, (c) S-18 and (d) S-19.

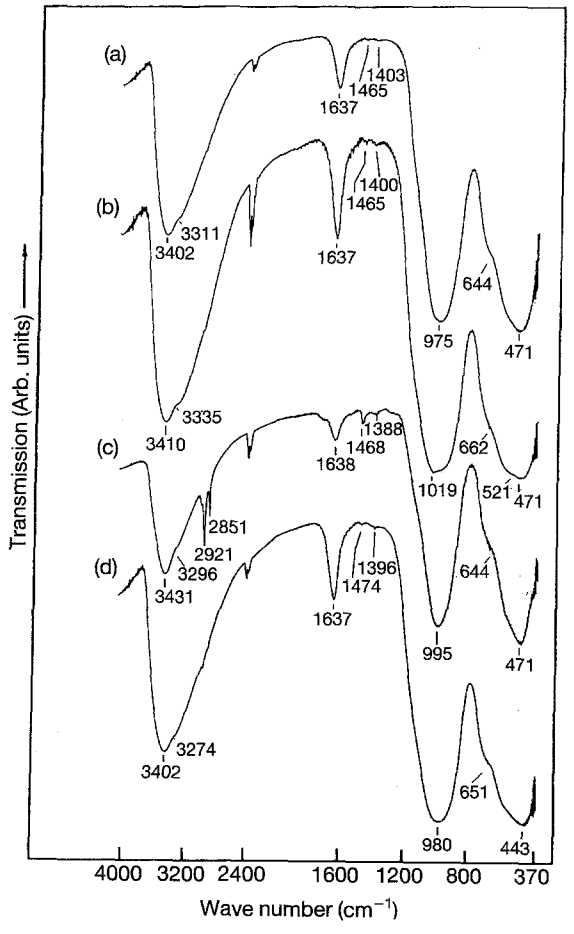

Figure 5 FT–IR spectra of corrosion products (a) S-12, (b) S-13, (c) S-14 and (d) S-15.

The results obtained in the present work by FT–IR spectroscopy indicated the ability of this technique to detect lepidocrocite and ferrihydrite in the rust, as well as other iron oxide phases. In the analysis of the rust, FT–IR spectroscopy can be used as a complementary technique to XRD and Mössbauer spectroscopy.

4. Discussion

The results of this study undoubtedly indicate the importance of temperature in the formation of ferrihydrite during the corrosion of steel in aqueous solutions. Ferrihydrite was detected only in the rust formed at 120 °C. The results also indicate that under given experimental conditions, the appearance of ferrihydrite in the rust was not dependent on the type of inorganic anion.

Generally, ferrihydrite is characterized by poor crystallinity, and it can transform to goethite and/or haematite. Foreign ions may affect this transformation. In the presence of divalent metal cations, ferrihydrite may transform into the ferrite phase. Cornell *et al.* [9] reported the transformation of ferrihydrite to lepidocrocite in slightly acidic solution under the influence of a reducing organic compound, L-cysteine, $HSCH_2CH(NH_2)COOH$.

XRD lines of ferrihydrite are broadened due to small crystallite sizes. Murad and Schwertmann [10] presented the Mössbauer spectra of ferrihydrate recorded at RT and 4 K. The fitting of the spectrum recorded at RT was performed for two doublets ($\Delta_1 = 0.54$ mm s^{-1}, and $\Delta_2 = 0.90$ mm s^{-1}). The Mössbauer spectrum of ferrihydrite, recorded at 4 K, showed hyperfine magnetic splitting with a wide distribution of hyperfine fields (average value near 500 kOe). Murad [11] supposed the existence of the tetrahedral and octahedral Fe^{3+} ions in ferrihydrite.

Carlson and Schwertmann [12] reported an IR band at 945–985 cm^{-1} for natural ferrihydrite. After the treatment of several ferrihydrite samples with NaOH, the intensity of this IR band decreased and its position was shifted to 930–945 cm^{-1}. After treatment of ferrihydrite samples with oxalate ions and HCl, the intensity of this IR band was additionally decreased and its position shifted to 1020–1070 cm^{-1}. A broad IR band between 900 and 1000 cm^{-1} was also observed for synthetic ferrihydrites prepared from the solutions containing Si^{4+} ions. The origin of this IR band was discussed in the sense of the vibrations of Si–O–Si and Si–O–Fe bonds [12].

The formation mechanism of ferrihydrite during the corrosion of steel is still unclear. It is generally accepted that iron hydroxy complexes formed after oxidation of Fe^0 are precursors of hydroxide and oxide phases. The crystal modifications of the oxide phases and their fractions in the rust are dependent on the conditions of the corrosion process. Fe^{3+} ions can be generated by the oxidation of Fe^{2+} or by dissolution of unstable oxide phases, for instance γ-FeOOH. A direct topotactic transformation of amorphous iron(III) hydroxide to ferrihydrite is not probable, if we know the fact that amorphous iron(III) hydroxide shows a certain structural similarity with lepidocrocite [13, 14]. It is more likely that ferrihydrite nucleates and grows inside the amorphous fraction.

Ferrihydrite is thermodynamically unstable and transforms into more stable phases with time, such as α-FeOOH and α-Fe_2O_3. Topotactic transformations, ferrihydrite → α-FeOOH→ α-Fe_2O_3, are possible because ferrihydrite and α-phases have a similar hexagonal close-packed anion sublattice. Ferrihydrite can transform directly to α-Fe_2O_3 at pH ≃ 7–8. These transformations are accelerated, if corrosion takes place at elevated temperature. During the corrosion process goethite can also be formed by the dissolution of lepidocrocite and the reprecipitation of α-FeOOH phase.

The formation of magnetite in the rust was often interpreted in the sense of decomposition of iron(II) hydroxide

$$3Fe(OH)_2 \rightarrow Fe_3O_4 + 2H_2O + H_2 \qquad (1)$$

However, if the corrosion of steel takes place in slightly acidic solutions, it is more likely that magnetite forms by the reaction of $FeOH^+$ complexes with Fe(III)-hydroxy complexes or amorphous iron(III) hydroxide. The reductive dissolution of γ-FeOOH may generate Fe^{2+} and Fe^{3+} ions in the form of hydroxy complexes, which may be precursors of magnetite. Ferrite phases, for instance $NiFe_2O_4$ and $CoFe_2O_4$, may also be formed, as corrosion products, by the reaction between amorphous iron(III) hydroxide and Ni^{2+} or Co^{2+} ions.

The influence of chlorides on the phase composition of the rust was studied by many authors. However, their results were very different. Therefore, in the present work particular attention was paid to that problem. Steel is often exposed to chlorides, for instance during the technical application of steel in the chemical industry, marine environment, etc. There is a relation between the appearance of stress corrosion cracking at elevated temperature and the concentration of chlorides and oxygen. This type of local corrosion occurs at a high concentration of oxygen and a low concentration of chlorides, or vice versa. Sea water is a very aggressive medium for steel surfaces, owing to a high concentration of NaCl and $MgCl_2$. Soils, which may contain a significant amount of chlorides, are also very aggressive media for steel surfaces.

Very thin iron foils were exposed to an atmosphere containing HCl and H_2O [15]. The Mössbauer spectrum of the rust showed a quadrupole doublet with parameters $\delta = 0.62$ mm s^{-1} (relative to sodium nitroprusside), and $\Delta = 0.64$ mm/s^{-1} (room temperature). These parameters were ascribed to $Fe(OH)_3$ and superparamagnetic Fe_2O_3.

The rust, formed after the exposure of steel plate to HCl fumes in air, was analysed by Mössbauer spectroscopy in backscattering or transmission arrangement [16]. Mössbauer parameters, measured for the rust at room temperature were $\delta = 0.64$ mm s^{-1} (relative to sodium nitroprusside), and $\Delta = 0.68$ mm s^{-1}. Hyperfine magnetic field with a value HMF = 468 kOe was observed at 80 K. These parameters were ascribed to β-FeOOH. The formation of β-FeOOH was also suggested on the basis of XRD.

The conversion electron Mössbauer spectrum (CEMS) of the iron surface, after its exposure to moist HCl gas for 2 h at room temperature, showed a central quadrupole doublet besides the lines of bulk iron [17]. Mössbauer parameters of the quadrupole doublet, $\delta_{Fe} = 1.18$ mm s^{-1} and $\Delta = 2.38$ mm s^{-1}, were ascribed to hydrous ferrous chloride. The spectrum of an iron foil, which was exposed to an atmosphere of moist HCl gas for 2 min and then to water vapour for 13 h, showed the quadrupole doublet with parameters $\delta_{Fe} = 0.38$ mm s^{-1} and $\Delta = 0.70$ mm s^{-1}. These parameters were ascribed to β-FeOOH.

The rust formed on the iron or steel surface, after its exposure to vapour above a HCl solution, was also analysed by Mössbauer spectroscopy [18]. A mixture of γ-FeOOH + β-FeOOH and, perhaps, of a small fraction of α-FeOOH was detected for concentrations from 0.1–3.5 HCl, while $FeCl_2 \cdot 4H_2O$ was detected for concentrations from 3.5–8.0 M HCl.

Corrosion of α-Fe was investigated in sea water and distilled, mineral or drinking water [19]. The corrosion products formed in sea water were identified as β-FeOOH, γ-FeOOH and FeOCl, while β-FeOOH was the dominant corrosion product in drinking water.

Meisel [20] found that the steel surface, after its exposure to HCl solutions for 4.5 years, contained γ-FeOOH, α-FeOOH and α-Fe_2O_3, whereas β-FeOOH was absent.

In the present work, the dependence of the corrosion of steel was investigated, on the concentration of chlorides, the type of cation (Na^+ or NH_4^+), temperature and the time of corrosion. β-FeOOH was not detected under given experimental conditions, either by XRD, or by FT–IR spectroscopy. It is possible with certainty to make a statement that the presence of chlorides during the corrosion of steel in an aqueous solution is not a dominant factor for the formation of β-FeOOH. We believe that the conclusions of other authors, concerning the formation of β-FeOOH in aqueous solution containing chlorides, are more based on the analogy with $FeCl_3$ hydrolysis than proved by experiments. An exception may be the formation of β-FeOOH in the rust in marine environments. It can be proposed that the first step of the corrosion process in a marine environment is the formation of $FeCl_3$, which further transforms to β-FeOOH by slow hydrolysis. The β-FeOOH transformation to other iron oxides depends on the wet/dry cycles. Probably, due to the facts just mentioned, some authors observed (or did not observe) β-FeOOH in the rust in marine environments. If detected, β-FeOOH was generally not a dominant component. Recently, we analysed several samples of the rust generated on the surface of powl bitts, taken in May 1991 at the Adriatic coast, and we could not detect β-FeOOH.

Formation of β-FeOOH on the iron surface, exposed to HCl + H_2O vapours, can be explained by a dissolution of iron during the first step of the corrosion process, which is followed by the formation of $FeCl_2/FeCl_3$ salts on the steel surface and with a further hydrolysis to β-FeOOH.

A significant effect of nitrate ions, in relation to other anions, on the composition of the rust was observed, when the corrosion process took place at 120 °C. The amorphous fraction was dominant in all corrosion products formed in the presence of nitrate ions at 120 °C, while ferrihydrite was an additional minor component. In corrosion product S-13, magnetite and haematite were also detected. Haematite probably crystallized directly from ferrihydrite.

The observed effect of nitrate ions on the corrosion process at 120 °C can be interpreted by the specific chemistry of these ions. In the absence of oxygen, NO_3^- reduces to NO_2^- by the reaction with nascent hydrogen, which is generated by the combination of the anodic reaction

$$Fe^0 - 2e^- = Fe^{2+}(aq) \quad (2)$$

and the cathodic reaction

$$2H^+(aq) + 2e^- = 2H \quad (3)$$

Further oxidation of Fe^{2+} ions generates Fe^{3+} ions which undergo hydrolysis and the precipitation of amorphous phase. It is known that NO_3^- ions can be used as an oxidizing agent for Fe^{2+} ions in the synthesis of magnetite or metal(II)-ferrites from Fe(II)-salt solutions as the starting material [21, 22]. All these reactions are accelerated at 120 °C. Nucleation and crystallization of ferrihydrite $Fe_5O_7(OH)\cdot 4H_2O$, take place inside the amorphous phase.

The analysis of the corrosion products formed in Na_2SO_4 solutions showed different phase composition, depending on the temperature of their formation. Corrosion products S-16 and S-17, formed at room temperature, contained lepidocrocite as the dominant component, while in corrosion products S-18 and S-19, formed at 120 °C, lepidocrocite was absent. This difference is a result of highly reductive conditions during the corrosion of steel in the autoclave at 120 °C. A certain analogy can be supposed with the phase composition if the rust formed by corrosion of steel in an SO_2/SO_3-rich atmosphere. In a previous paper [1] we showed that γ-FeOOH, α-FeOOH and γ-Fe_2O_3 (or substoichiometric magnetite, $Fe_{3-x}O_4$) are typical corrosion products of steel during the corrosion of steel in an SO_2/SO_3-rich atmosphere. The kinetics of transformation of the early corrosion product, γ-FeOOH, to the final product, γ-Fe_2O_3, was determined. The formation of α-FeOOH was explained by the mechanism of γ-FeOOH dissolution and α-FeOOH reprecipitation.

On the other hand, different results were obtained when the atmospheric corrosion of iron (steel) was simulated in the laboratory [23]. In a highly SO_2-polluted atmosphere, basic iron(III) sulphate was identified as an early corrosion product. After 3 months corrosion, only γ-FeOOH was found in the rust. It was also shown under laboratory conditions that the concentration of SO_2 plays a significant role in the formation of Fe^{2+} species, during the corrosion of iron or weathering steel [24].

References

1. H. LEIDHEISER Jr. and S. MUSIĆ, *Corrosion Sci.* **22** (1982) 1089.
2. H. LEIDHEISER Jr. and I. CZAKÓ-NAGY, *ibid.* **24** (1984) 569.
3. H. LEIDHEISER Jr, S. MUSIĆ and J. F. McINTYRE, *ibid.* **24** (1984) 197.
4. S. MUSIĆ, A. VÉRTES, G. W. SIMMONS, I. CZAKÓ-NAGY and H. LEIDHEISER, Jr, *J. Coll. Interface Sci.* **85** (1982) 256.
5. S. MUSIĆ, I. CZAKÓ-NAGY, S. POPOVIĆ, A. VÉRTES and M. TONKOVIĆ, *Croat, Chem. Acta* **59** (1986) 833.
6. S. MUSIĆ, S. POPOVIĆ and M. GOTIĆ, *ibid.* **60** (1987) 661.
7. *Idem, J. Mater. Sci.* **25** (1990) 3186.
8. International Centre for Diffraction Data, Joint Committee on Powder Diffraction Standards, Powder Diffraction File, 1601 Park Lane, Swarthmore, PA 19081, USA.
9. R. M. CORNELL, W. SCHNEIDER and R. GIOVANOLI, *Clay Miner.* **24** (1989) 549.
10. E. MURAD and U. SCHWERTMANN, *Am. Miner.* **65** (1980) 1044.
11. E. MURAD, *J. Magn. Magn. Mater.* **74** (1988) 153.
12. L. CARLSON and U. SCHWERTMANN, *Geochim. Cosmochim. Acta* **45** (1981) 421.
13. M. KOBAYASHI and M. UDA, *J. Non-Cryst. Solids* **29** (1978) 419.
14. *Idem, ibid.* **41** (1980) 241.
15. D. D. JOYE and R. C. AXTMANN, *Anal. Chem.* **40** (1968) 876.

16. J. H. TERRELL and J. J. SPIJKERMAN, *Appl. Phys. Lett.* **13** (1968) 11.
17. M. J. TRICKER, J. M. THOMAS and A. P. WINTERBOTTOM, *Surface Sci.* **45** (1974) 601.
18. V. RAMSHESH, K. RAVICHANDRAN and K. S. VENKATESWARLU, *Ind. J. Chem.* **20A** (1981) 867.
19. T. PÉEV, M. K. GEORGIEVA, S. NAGY and A. VÉRTES, *Radiochem. Radioanal. Lett.* **33** (1978) 265.
20. W. MEISEL, *J. Phys. (Fr.)* **41** (1981) C1-63.
21. T. SUGIMOTO and E. MATIJEVIĆ, *J. Coll. Interface Sci.* **74** (1980) 227.
22. Z. X. TANG, C. M. SORENSEN, K. J. KLABUNDE, G. C. HADJIPANAYIS, *ibid.* **146** (1991) 38.
23. J. R. GANCEDO and M. L. MARTINEZ, in "Magnetic Resonance in Colloid and Interface Science", edited by J. P. Fraissard and H. A. Resing (D. Reidel, 1980) p. 371–6.
24. J. R. GANCEDO, M. GRACIA, J. F. MARCO and J. PALACIOS, *Hyperfine Interact.* **41** (1988) 637.

Received 15 May 1992
and accepted 5 March 1993